

# Renewable Energy Research and Applications (RERA)



Vol. 6, No. 2, 2025, 284-292

DOI: 10.22044/rera,2025.16314.1424

# A Bidirectional On-Board Integrated EV Charger with Flexible Input Sources and Direct Renewable Energy Connection Capability

M. Khakpour<sup>1</sup>, Y. Karimi<sup>1\*</sup> and M. H. Zare<sup>2</sup>

1. Electrical Engineering Department, Yazd University, Yazd, Iran. 2. Faculty of Engineering, Ardakan University, Ardakan, Iran.

Received Date 28 May 2025; Revised Date 11 August 2025; Accepted Date 24 September 2025 \*Corresponding author: karimiyaser@yazd.ac.ir (Y. Karimi)

### **Abstract**

To address key challenges in the widespread adoption of electric vehicles, this article introduces a bidirectional, integrated on-board battery charger capable of flexibly drawing power from various AC sources, such as single-phase and three-phase grids, as well as renewable energy DC sources like photovoltaic (PV) energy systems. The charger is designed for vehicles with an open-end winding motor powered by a dual inverter, consisting of two three-phase traction inverters and two sets of batteries. The proposed design utilizes a bidirectional current source converter at the input stage and integrates the dual inverter and the motor windings' leakage inductance as part of the charger, reducing both size and cost. Operating bidirectionally, the charger supports various grid support strategies, offering controlled active and reactive power with low total harmonic distortion (THD) in the grid current. It can also be directly connected to PV panels or DC fast-charging stations. A zero-net-torque-generating, interleaved switching pattern is employed to control the dual inverter switches, minimizing current ripple throughout the system. This article provides a detailed explanation and analysis of the proposed integrated charger, with system feasibility and performance validated through simulations.

**Keywords:** Electric Vehicle (EV), Integrated On-Board Charger (IOBC), Bidirectional Current Source Converter (B-CSC), Dual Inverter Drive, Open-End Winding Machine, Renewable Energy Source.

### 1. Introduction

The decline of fossil fuel reserves and rising environmental concerns have accelerated the global shift toward electric vehicles (EVs). EVs offer a sustainable alternative to conventional vehicles by reducing greenhouse gas emissions, especially when charged through renewable energy sources [1,2]. However, their large-scale adoption faces key obstacles such as high costs, limited charging infrastructure, long charging durations, and battery lifespan [3].

Electric vehicle (EV) charging systems are classified into two main categories: on-board and off-board chargers. Off-board chargers, located externally at dedicated charging stations, deliver high power to reduce charging time, though they require substantial infrastructure investment. In contrast, on-board chargers are integrated into the vehicle and often leverage existing subsystems—such as the traction inverter, thermal management system, and electric motor—to facilitate energy transfer during the charging process while the EV is parked. This integration can significantly

decrease both system volume and associated costs [4,5]. The topology introduced in [6] employs a front-end power factor correction (PFC) boost converter interfaced with a single-phase grid, and utilizes the traction inverter and three-phase motor as parts of the charger. However, this approach necessitates access to the motor's neutral point and is constrained by the inherent limitations of single-phase PFC converters. Alternatively, openend winding machines driven by dual inverters have gained considerable attention due to their advantages, including an inherent multilevel converter structure, reduced current ripple in the motor windings, and the capability to drive highvoltage motors using dual inverters powered by independent sets of low-voltage batteries [7].

In [8], a charger topology is proposed that utilizes the dual-inverter configuration and the leakage inductances of an open-end winding machine to enable battery charging via a DC microgrid. Building upon this concept, [9] extends the architecture by incorporating two additional halfbridges as grid interface stages, thereby enabling operation from a single-phase grid. While threephase sources support high-power energy transfer for charging, preventing torque generation during charging remains a critical constraint for most three-phase integrated chargers, whether for chargers employing three-phase electrical machines [10] or their multi-phase counterparts, including six-phase [11] and five-phase [12] topologies. Various implementations address this issue through the inclusion of auxiliary mechanical components, such as clutches or rotor locking mechanisms, to mitigate unintended during charging. torque production approaches employ mechanical switches to reconfigure stator windings, facilitating connection to the three-phase grid while suppressing undesired torque. However, these methods can degrade system performance, introduce mechanical wear, increase spatial requirements, and potentially reduce long-term reliability [13]. The three-phase charger topology presented in [14] integrates a current source converter (CSC) for AC/DC conversion with a dual-inverter drive. This design offers benefits such as reduced current ripple magnitude and higher ripple frequency, allowing for more compact LC filtering. Nevertheless, it operates unidirectionally and lacks support for Vehicle-to-Grid (V2G) functionality. To enable bidirectional operation, [15] proposes a polarity inversion module, which may reduce overall system reliability.

This paper presents a bidirectional three-phase integrated on-board charger topology featuring flexible input sources and direct integration with renewable energy systems, based on a dual-inverter drive. The dual-inverter effectively reduces current ripple, allowing for a more compact LC filter design on the grid side and reducing the need for extensive motor winding

inductance. The incorporated bidirectional current source converter (B-CSC) offers several benefits, including power factor correction, rapid dynamic response, and improved waveform quality. The topology supports bidirectional power flow across all power factors, enabling V2G functionality. This facilitates multiple grid services such as reactive power support for voltage regulation, load leveling, peak shaving, frequency stabilization, and backup power supply during grid outages. Additionally, the system can switch off all B-CSC switches and operate via the dual inverter for motor operation in propulsion mode.

The proposed charger can be flexibly connected to single-phase and three-phase grids, as well as DC sources such as DC fast-charging stations, DC microgrids, and renewable energy sources like photovoltaic (PV) systems. PV can be directly connected to the proposed charger without the need for an external Maximum Power Point Tracking (MPPT) stage due to the built-in MPPT algorithm.

The system operating and control principles and charger design are detailed in Section 2, Section 3 presents the simulation results, and Section 4 provides the conclusions.

## 2. System operation

Figure 1 Shows the structure of the proposed integrated charger, which consists of a bidirectional current source converter, an LC filter, two traction inverters, an open-end winding motor, and two identical battery packs. Notably, the design can accommodate hybrid energy storage configurations, such as combined battery-supercapacitor systems. During charging, the dual inverters function as a pair of DC/DC converters to manage battery charging, while in propulsion mode, they operate as DC/AC converters to drive the motor.

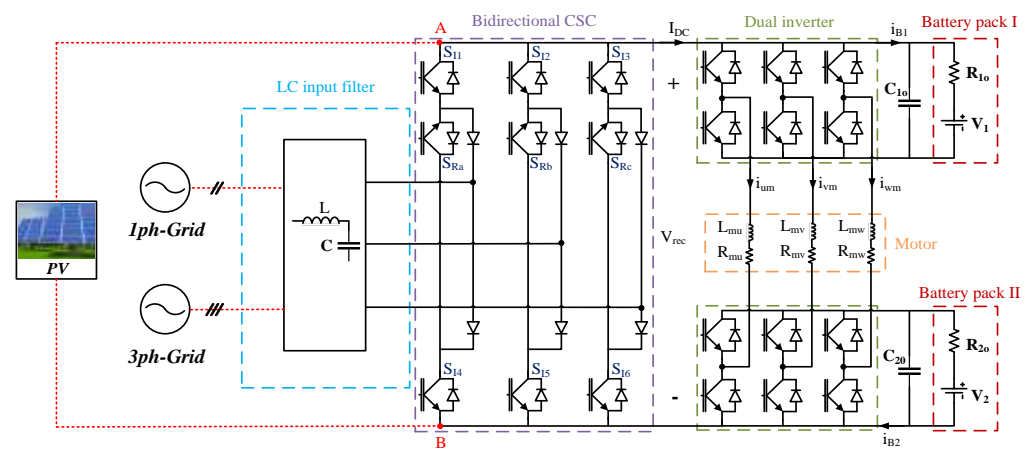


Figure 1. The proposed bidirectional integrated charger with flexible input sources

The AC outputs of the inverters connect directly to the motor's open-end windings, with the motor's leakage inductance shared between the two inverter networks, thereby eliminating the need for additional magnetic components in the charging circuit. The use of dual traction inverters reduces current ripple and uses differential connections for enhanced EV charging performance. This section presents a detailed analysis of the system's operating and control principles, including the B-CSC, dual inverters, and the filter.

# 2.1. B-CSC operating principles

In contrast to three-phase voltage source converters (VSCs), three-phase current source converters (CSCs) provide a wider output voltage range, reduced inrush current during start-up, and inherent short-circuit current limitation. These characteristics make CSCs particularly suitable for applications involving high-voltage input and high-current, low-voltage output, such as in telecommunication power supplies and electric vehicle on-board chargers where efficiency and grid current quality are critical performance metrics [16].

The modulation of the B-CSC requires continuous current flow through the DC-link, as any interruption can lead to voltage spikes across the DC-link. While several modulation methods exist for B-CSCs, the current space vector modulation (CSVM) method will be used for the proposed charger because CSVM is simple to implement and provides fast dynamic response for control of grid current magnitude and phase angle [17].

CSVM shapes the input current by nine permissible switching states—six active and three zero vectors—distributed across six symmetrical sectors in the complex plane. The incoming three-phase current to the B-CSC is controlled to track a reference current vector  $\bar{I}$ , defined as:

$$\vec{\bar{I}} = \bar{I} \begin{bmatrix} \cos \bar{\Theta} \\ \sin \bar{\Theta} \end{bmatrix} \tag{1}$$

in which  $\bar{I}$  denotes the magnitude and  $\bar{\theta}$  represents the phase angle of the current vector  $\vec{I}$ . Within a single sampling cycle,  $\vec{I}$  is synthesized using two active vectors and one zero vector. As an illustrative case, the corresponding duty ratios are presented for Sector I; due to the system's symmetry, the same approach can be extended to all other sectors. In sector I, shaping  $\vec{I}$  is achieved by sequentially switching the B-CSC to the  $I_1$  vector for  $T_1$ , the  $I_2$  vector for  $T_2$ , and the  $I_0$  vector

for  $T_0$ , all within one B-CSC switching period. The duty ratio expressions are derived as follows:

$$T_1 = M_I T_{S-BCSC} \sin \left( \frac{\Pi}{6} - \bar{\Theta} \right)$$
 (2)

$$T_2 = M_I T_{S-BCSC} SIN \left( \frac{\Pi}{6} + \bar{\Theta} \right)$$
 (3)

$$T_0 = T_{s-BCSC} - T_1 - T_2 (4)$$

FOR 
$$-\frac{\pi}{6} \le \bar{\Theta} \le \frac{\pi}{6}$$
 (5)

The parameter  $M_i$  denotes the B-CSC modulation index while  $T_{s-BCSC}$  stands for one switching period of the B-CSC. The selected switching pattern is specifically designed to minimize current ripple and reduce the switching frequency within each cycle, thereby lowering overall power losses [18].

The B-CSC used in the proposed charger topology integrates a three-phase current source inverter (3ph-CSI) and a three-phase three-switch current source rectifier (3ph-CSR) [19]. This configuration supports bidirectional operation, functioning either as a rectifier enabling G2V mode or as an inverter enabling V2G mode. Switch conduction patterns required to achieve each vector for both V2G and G2V modes are outlined in [20]. CSVM scheme is illustrated in the  $\alpha\beta$  reference in figure 2.

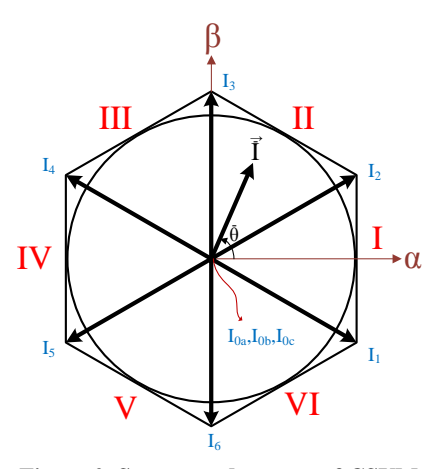


Figure 2. Sectors and vectors of CSVM

## 2.2. Dual-Inverter operating principles

Charger architectures employing a single battery and one inverter per motor are constrained in grid voltage compatibility, as the battery's minimum state of charge must exceed the peak amplitude of the grid AC voltage. Alternatively, dual-inverter configurations enable the use of higher-voltage motors by leveraging two conventional low-voltage inverters, thereby enhancing overall system efficiency, improving compatibility with grid voltage levels, and mitigating harmonic

distortion and  $\frac{dv}{dt}$  induced stress [21]. This configuration integrates an open-end winding machine between dual traction inverters, leveraging the motor's leakage inductance as an effective filtering element. Due to the constraints imposed by the motor's magnetic design on available leakage inductance, advanced control techniques are required to suppress highfrequency ripple components. To address this, two distinct modulation strategies are applied. One of these involves phase-interleaved switching known as inter-winding interleaving, where the carrier signals of the inverter half-bridges are offset by one-third of the submodule switching period This coordination enables bidirectional converter to operate at harmonic frequencies aligned with integer multiples of  $\frac{T_{s-dinv}}{3}$ , resulting in reduced current ripple within the DC-link and more stable charging currents to the battery system. Another advanced modulation method, referred to as inter-inverter interleaving, introduces a temporal shift of  $\frac{T_{s-dinv}}{2}$  between the switching carriers of the half-bridges in the two inverters. This synchronization forces the system to operate at harmonic intervals aligned with integer multiples of  $\frac{T_{s-dinv}}{2}$ , effectively reducing ripple in both the DC-link and motor phase currents. When combined with inter-winding interleaving, the benefits of both techniques are

simultaneously realized. Under this dual-interleaving scheme, the switching cycle becomes  $\frac{T_{s-dinv}}{6}$ , ensuring consistent and periodic current sampling. This results in a higher effective switching frequency, which suppresses grid-side harmonic emissions and may allow for smaller input filter. Additionally, it reduces the switching requirements of the main traction inverters while maintaining a sinusoidal current waveform in the machine [22]. A detailed overview of these interleaving strategies and their benefits is presented in Table 1.

The proposed topology confines current flow within the machine windings exclusively to zero-sequence components, thereby eliminating torque production. To maintain this condition, the operational states of all phases in the traction inverters must remain precisely identical. The duty cycles associated with the applied switching patterns are specified in [23]. As shown in figure 1, the upper and lower traction inverters are arranged.

The dual inverters are connected in series, allowing the charger to utilize the combined voltage of both battery packs. This design overcomes the voltage limitations inherent in single-battery systems and enables effective interfacing with higher-voltage systems, enhancing the flexibility and scalability of the onboard charging system.

Inter-winding	Inter-inverter	Maximum operable f <sub>s-BCSC</sub>	Current ripple mitigation
Not adopted	Not adopted	$f_{s-dinv}$	None
Adopted	Not adopted	$3f_{s-dinv}$	$I_{DC}$ , $i_{B1}$ , $i_{B2}$
Not adopted	Adopted	$2f_{s-dinv}$	$I_{DC}$ , $i_{um}$ , $i_{vm}$ , $i_{wm}$
Adopted	Adopted	$6f_{s-dinv}$	$I_{DC}$ , $i_{um}$ , $i_{vm}$ , $i_{wm}$ , $i_{B1}$ , $i_{B2}$

Table 1. detailed overview of dual inverter interleaved switching strategies

## 2.3. Grid-Side LC filter design

The filter design of the B-CSC is mainly determined by the allowable limits on the grid current THD and input voltage distortion. The switching operations within the B-CSC generate high-frequency harmonic components in the line currents, which can be effectively suppressed by using a passive LC filter. In this study, a filter design based on CSVM is presented to extract smooth, sinusoidal currents from the grid. To improve system stability and dampen oscillations at the LC resonant frequency, damping resistors are connected in parallel with the filter inductors. Although virtual damping methods offer a lossless alternative, they require additional computational effort and more advanced sensing capabilities [24].

A frequency domain analysis of the B-CSC is conducted to inform the filter design process. The LC filter parameters are determined through an analytical evaluation of the input current ripple, ensuring that the RMS magnitude of the grid current ripple remains within prescribed limits to achieve the desired THD. According to IEEE 519, the THD of the grid current must not exceed 5% frequency its fundamental component. Additionally, for optimal B-CSC performance, the input voltage should exhibit minimal high-order harmonic content. Achieving efficient operation requires the extraction of grid current with a power factor approaching unity, while minimizing the fundamental frequency voltage drop across the input filter. The LC filter parameters are determined by applying the design equations outlined in [25], which incorporate the specified limits on current ripple, harmonic distortion, and voltage drop, ensuring that the filter design aligns with relevant standards.

## 2.4. Direct PV connection and MPPT

PV panels can be directly connected to the proposed charger without the need for an external converter for MPPT. This connection can be implemented in two ways: by connecting the PV panels to two phases of the B-CSC input and turning on corresponding phase-specific switches, or by bypassing the B-CSC and directly connecting to the DC-link terminals (points A and B in Figure 1). While bypassing the B-CSC can reduce conduction losses in the semiconductor switches, it requires an additional terminal for connection. Furthermore, this configuration makes it infeasible to use the input LC filter, which is typically employed to reduce PV current ripple. Figure 3 illustrates the MPPT control loop for direct PV connection, which determines the DClink current reference value ( $I_{DC-ref}$ ). MPPT can be implemented using common techniques such as Perturb and Observe (P&O). Incremental Conductance, or advanced methods like Global Maximum Power Point Tracking (GMPPT) strategies to handle partial shading conditions [26]. In the proposed system, the state of charge (SoC) of the battery is integrated into the MPPT algorithm. The tracking process is halted operational limit—such whenever any maximum SoC, battery current, or battery voltage—is reached. Otherwise, the system continues to extract and deliver the maximum available PV power to the batteries.

# 2.5. Control principles

This study initially considered an idealized symmetrical system with balanced energy sources, enabling the controller to apply identical duty cycles to both the upper and lower power traction inverters. To manage scenarios in which the battery packs possess different state of charges during charging, the duty cycles are decomposed into sum and difference components. This charger is designed to regulate the DC inductor current through the sum component, while the difference component facilitates the equalization of stored energy between the split energy sources.

# 2.5.1. Inductor current control

As shown in Figure 3, three PI controllers are employed to regulate the current in parallel phases, ensuring constant current operation. Since the DC current at the vehicle inlet is typically managed, each inductor current is set to track onethird of the total DC bus current reference. The system dynamics are formulated by expressing the duty cycles in terms of their sum (D) and difference ( $\Delta d$ ), as defined in [27]. Ideally, when battery voltages are balanced, the DC current is controlled predominantly by the sum component. However, the difference component remains coupled to the current controller. To maintain stability, the voltage balancing controller is designed with a slower response relative to the current controller, allowing the term (V1- V2) Δd to be considered as a quasi-static offset within the current control timeframe.

## 2.5.2. Energy balancing

As illustrated in Figure 3, the voltage balancing controller processes the voltage difference between the two sources and generates the differential duty term  $\Delta d$ . This strategy ensures that when the upper.

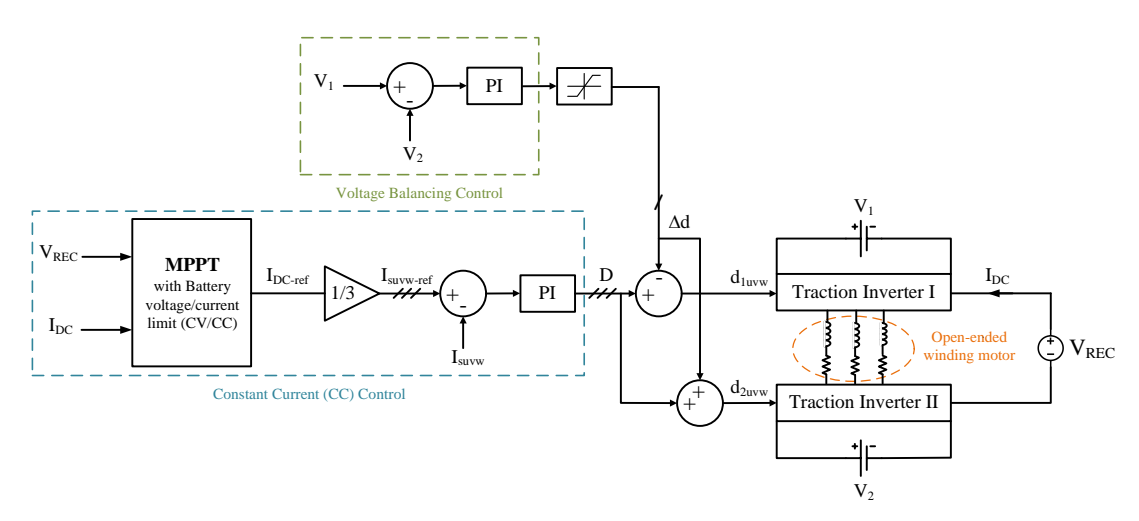


Figure 3. charger full control strategy.

As illustrated in Figure 3, the voltage balancing controller processes the voltage difference between the two sources and generates the differential duty term  $\Delta d$ . This strategy ensures that when the upper battery pack is more charged than the lower one, the lower traction inverter is switched more frequently, redistributing power to balance the energy levels. Although both battery packs are charged concurrently, the introduction of this offset shifts the power flow to correct the imbalance. To prevent the differential duty adjustment from exceeding the converter's operational constraints, a limiter is applied at the output of the voltage balancing controller [28].

### 3. Simulation results

A full-switch model of the proposed integrated charger, with the parameters provided in Table 2, was developed and simulated in MATLAB/Simulink. The simulation outcomes confirm the following:

• Effective MPPT implementation for the PV system.

- Current control functionality.
- Zero average torque production while charging.
- Current ripple reduction through the proposed interleaved switching.
- Supporting G2V and V2G operating modes

The P&O algorithm is one of the most widely used strategies for MPPT, owing to its algorithmic simplicity and reliable tracking performance. This approach works by slightly changing the PV system's current and then observing how the output power responds. This change in power is compared to the previous value to determine whether the system is moving toward or away from the maximum power point (MPP). This power variation is compared against its prior value to infer the direction of system response. A positive differential suggests motion toward MPP, justifying a continuation of the perturbation in the same direction.

Tabla	2	Creators	Parameters	
i anie	Z.,	System	Parameters	3

System parameter	Symbol	Value
Motor winding leakage inductance	$L_{um}, L_{vm}, L_{wm}$	0.5 mΩ
Motor winding resistance	$R_{um}$ , $R_{vm}$ , $R_{wm}$	55 mΩ
Dual inverter switching frequency	$f_{s-dinv}$	10 kHz
DC-link capacitance	$C_{1o}$ , $C_{2o}$	4.9 mF
Battery internal resistance	$R_{1o}, R_{2o}$	48 mΩ
Filter inductance	L	32.6 μΗ
Filter capacitance	С	63 μF
Filter damping resistance	$R_{damp}$	150 Ω
PV maximum power	$P_{mpp}$	8.82 kW
PV voltage at maximum power	$V_{mpp}$	363.6 V
PV short circuit current	$I_{sc}$	8.61 A
PV temperature	Тетр	25 °C
PV open circuit voltage	$V_{oc}$	37.4 V

In contrast, a negative differential implies deviation from the MPP, prompting a reversal of the perturbation direction. This iterative process is sustained until the power differential term approaches zero, signifying that the system has reached the MPP. With changes in irradiance while the temperature remains constant, the output current of the PV system varies according to the characteristic curve depicted in figure 4.

As shown in figure 5, the output power also changes proportionally with irradiance, and the MPP is effectively tracked.

Figure 6 illustrates the dynamic system response to a step change in current applied at t = 1.5 s, where the inductor reference current is increased from 7A to 9A. This adjustment results in a corresponding rise in total input power, DC bus

current, and the current supplied to the battery packs.

D initially decreases to accommodate the increased current demand and stabilizes at its new steady-state value. Thus, the constant current control strategy effectively manages dynamic changes, ensuring rapid stabilization of system variables.

Figure 7(b) shows the DC link current obtained using both interleaving methods, while Figure 7(a) shows the DC link current obtained using both interleaving methods current waveforms without interleaved switching for comparison. Under the interleaved switching condition, the harmonic reduction of the DC link current is confirmed.

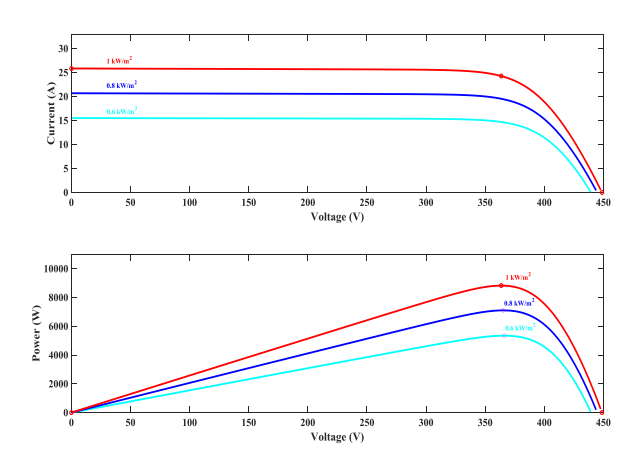


Figure 4. I\_V and P\_V characteristics of PV in variable irradiance and constant temperature.

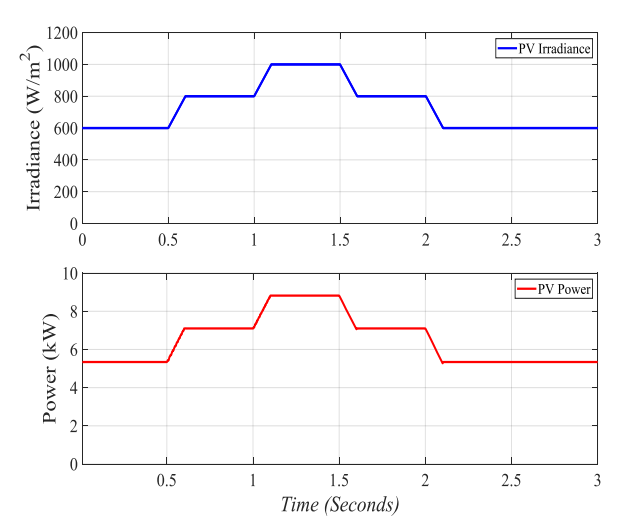


Figure 5. Variable irradiance scenario and PV power.

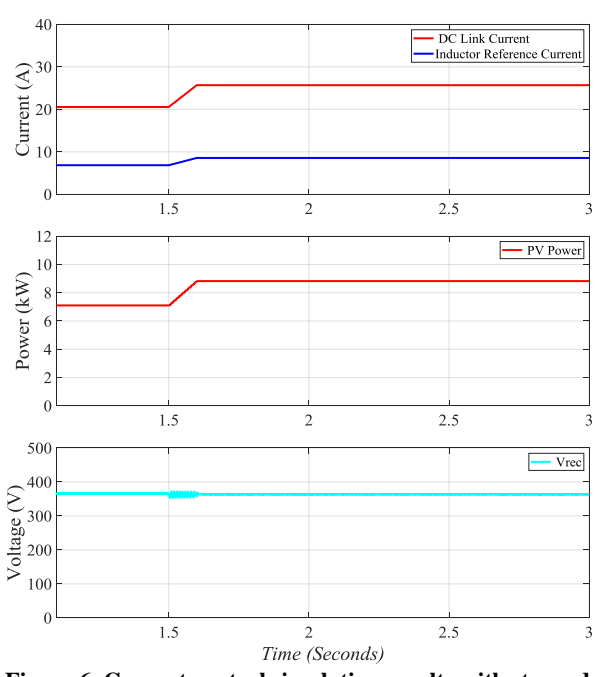


Figure 6. Current control simulation results with stepped inductor reference current

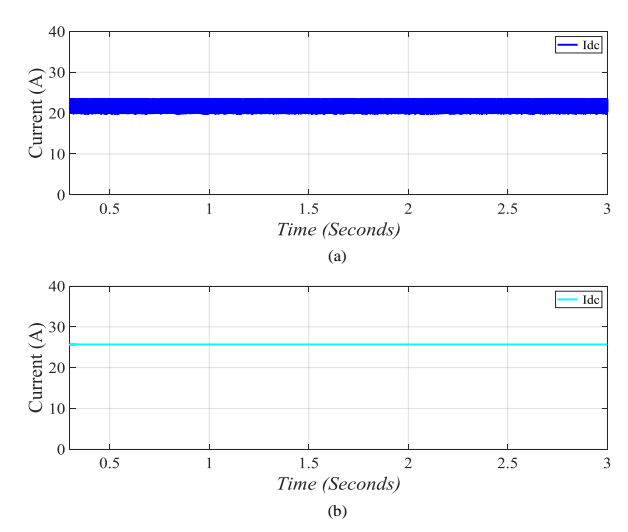


Figure 7. DC link current ripple in (a) conventional switching and (b) both interleaved switching

For a symmetrical machine, the phase currents are identical. Figure 8 shows that the motor currents constitute a zero-sequence set, which leads to zero average torque production by the machine. Figure 9 illustrates bidirectional power flow functionality of the charger when connected to a 3ph AC source, enabling not only energy transfer to the EV but also reverse power delivery to the grid. This allows the charger to provide grid services. Moreover, the topology operates at near-unity power factor, achieving a grid-side power factor greater than 0.995. It also complies with the IEEE 519 standard for grid harmonics, with THD levels of 2.8% in G2V mode and 0.79% in V2G mode.

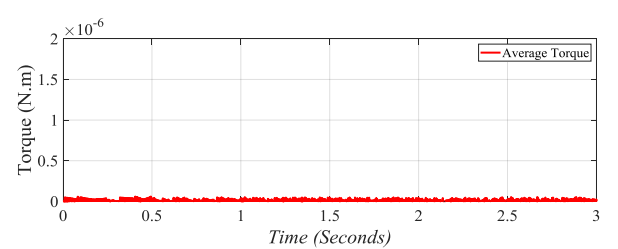
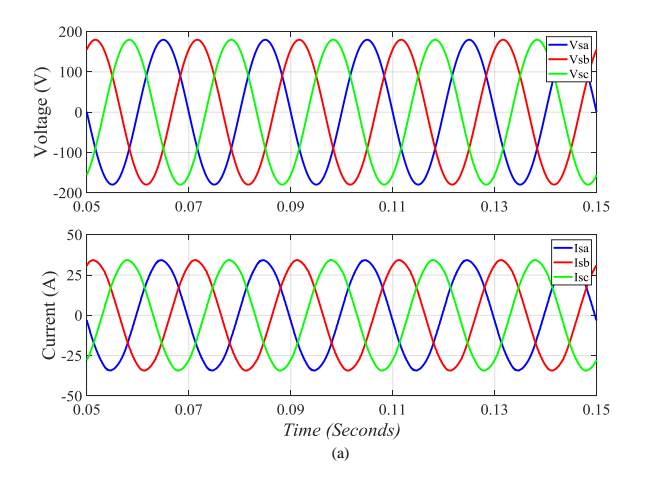


Figure 8. Motor torque production while charging



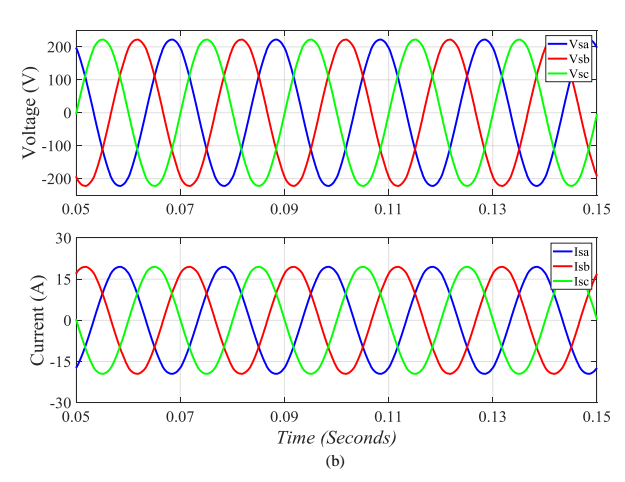


Figure 9. Three phase grid voltage and current in (a)G2V and (b)V2G modes of operation.

#### 4. Conclusion

This paper presented a bidirectional integrated onboard charger for EVs that supports the capability to flexibly draw power from various AC and DC sources, including direct PV connections. By leveraging a dual-inverter, open-end winding machine configuration, and B-CSC, the proposed design enables efficient power conversion with reduced current ripple, minimized production during charging, and enhanced grid compatibility. The use of the B-CSC ensures highquality grid interaction with inherent current limiting, low total harmonic distortion, and full V2G capability.

Additionally, the built-in MPPT control allows direct PV integration without external DC-DC converters, further increasing system efficiency and reducing cost. Simulation results validate the effectiveness of the proposed system in maintaining stable current control, ensuring battery voltage balancing, suppressing ripple currents, and accurately tracking the MPP in PV mode. The presented charger topology is an efficient, highly integrated, scalable, and reliable solution for next-generation EV chargers, particularly in smart-grid and renewable-powered scenarios.

# 5. Acknowledgement

The authors would like to acknowledge the use of AI-assisted tools (such as ChatGPT) for improving the clarity and grammar of the manuscript.

## 6. References

[1] Ghaedi, A., Mahmoudian, M. and Sedaghati, R. (2022). Reliability Modeling of Different Types of Electric Vehicles in Renewable Applications. Renewable Energy Research and

- Applications, 3(2), 255-266. doi: 10.22044/rera.2022.11711.1103.
- [2] Babaie Pirouziana, A. R., Zahedi, R., Ahmadi, A. and Olya, N. (2023). Integration of Renewable Energy-Based Systems for Transport Sector in 2050; a Case Study in Iran. Renewable Energy Research and Applications, 4(1), 21-30. doi: 10.22044/rera.2022.11910.1124.
- [3] M. Yilmaz and P. T. Krein, "Review of Battery Charger Topologies, Charging Power Levels, and Infrastructure for Plug-In Electric and Hybrid Vehicles," in IEEE Transactions on Power Electronics, vol. 28, no. 5, pp. 2151-2169, May 2013, doi: 10.1109/TPEL.2012.2212917.
- [4] Nasr Esfahani, F., Darwish, A., Ma, X., & Twigg, P. (2024). Non-Integrated and Integrated On-Board Battery Chargers (iOBCs) for Electric Vehicles (EVs): A Critical Review. Energies.
- [5] Dehghanmongabadi, A. and Tahmasbnia, Z. (2025). Sustainable Development Indicators and Solutions in the Urban Transportation Sector with Emphasis on the use of Renewable Energies Based on the Scoping Review Method. Renewable Energy Research and Applications, 6(1), 125-137. doi: 10.22044/rera.2024.14255.1298.
- [6] Verma, P., Gangal, B., Jain, G. and Hada, R. (2024). A New Global Maximum Power Point Algorithm for Dynamic Shading Patterns of Partial Shading. Renewable Energy Research and Applications, 5(2), 211-220. doi: 10.22044/rera.2023.12408.1180.
- [7] J. Hong, H. Lee and K. Nam, "Charging Method for the Secondary Battery in Dual-Inverter Drive Systems for Electric Vehicles," in IEEE Transactions on Power Electronics, vol. 30, no. 2, pp. 909-921, Feb. 2015, doi: 10.1109/TPEL.2014.2312194.
- [8] R. Shi, S. Semsar and P. W. Lehn, "Constant Current Fast Charging of Electric Vehicles via a DC Grid Using a Dual-Inverter Drive," in IEEE Transactions on Industrial Electronics, vol. 64, no. 9, pp. 6940-6949, Sept. 2017, doi: 10.1109/TIE.2017.2686362.
- [9] S. Semsar, T. Soong and P. W. Lehn, "On-Board Single-Phase Integrated Electric Vehicle Charger With V2G Functionality," in IEEE Transactions on Power Electronics, vol. 35, no. 11, pp. 12072-12084, Nov. 2020, doi: 10.1109/TPEL.2020.2982326.
- [10] M. Tong, M. Cheng, S. Wang and W. Hua, "An On-Board Two-Stage Integrated Fast Battery Charger for EVs Based on a Five-Phase Hybrid-Excitation Flux-Switching Machine," in IEEE Transactions on Industrial Electronics, vol. 68, no. 2, pp. 1780-1790, Feb. 2021, doi: 10.1109/TIE.2020.2988242.
- [11] H. J. Raherimihaja, Q. Zhang, T. Na, M. Shao and J. Wang, "A Three-Phase Integrated Battery Charger for EVs Based on Six-Phase Open-End Winding

- Machine," in IEEE Transactions on Power Electronics, vol. 35, no. 11, pp. 12122-12132, Nov. 2020, doi: 10.1109/TPEL.2020.2986798.
- [12] I. Subotic, N. Bodo and E. Levi, "An EV Drive-Train With Integrated Fast Charging Capability," in IEEE Transactions on Power Electronics, vol. 31, no. 2, pp. 1461-1471, Feb. 2016, doi: 10.1109/TPEL.2015.2424592.
- [13] H. J. Raherimihaja, G. Xu and Q. Zhang, "Review and Novel Options of Three-Phase Integrated Battery Chargers for EVs," 2020 IEEE Vehicle Power and Propulsion Conference (VPPC), Gijon, Spain, 2020, pp. 1-5, doi: 10.1109/VPPC49601.2020.9330895.
- [14] S. Wang and P. W. Lehn, "A Three-Phase Electric Vehicle Charger Integrated With Dual-Inverter Drive," in IEEE Transactions on Transportation Electrification, vol. 8, no. 1, pp. 82-97, March 2022, doi: 10.1109/TTE.2021.3102192.
- [15] S. Wang and P. W. Lehn, "Design and Control of 3-Phase Integrated Charger for Dual-Inverter Drivetrain Electric Vehicles," 2019 IEEE Transportation Electrification Conference and Expo (ITEC), Detroit, MI, USA, 2019, pp. 1-6, doi: 10.1109/ITEC.2019.8790589.
- [16] Q. Zhang, M. Shao, Z. Wei and H. Guang, "A Study of Charging Equivalent Inductances for Zero-Average-Torque Three-Phase-Integrated On-Board EV Chargers With Segmented Machine," in IEEE Transactions on Power Electronics, vol. 38, no. 12, pp. 15442-15455, Dec. 2023, doi: 10.1109/TPEL.2023.3314794.
- [17] B. Wu, High-Power Converters and AC Drives. Hoboken, NJ, USA: Wiley, 2006, pp. 189–249.
- [18] Q. Chen, S. Su, X. Zhang, M. Ma and F. Li, "Three-Phase Current Source Rectifier With Reduced Voltage Stress on Switching Devices and Common Mode Current Mitigation," in IEEE Transactions on Industry Applications, vol. 60, no. 2, pp. 3018-3028, March-April 2024, doi: 10.1109/TIA.2023.3344089.
- [19] V. Vekhande, K. V. K. and B. G. Fernandes, "Control of Three-Phase Bidirectional Current-Source Converter to Inject Balanced Three-Phase Currents Under Unbalanced Grid Voltage Condition," in IEEE Transactions on Power Electronics, vol. 31, no. 9, pp. 6719-6737, Sept. 2016, doi: 10.1109/TPEL.2015.2503352.
- [20] M. Khakpour and Y. Karimi, "A Bidirectional Three-Phase on-Board Integrated EV Charger Employing Dual-Inverter Drive," 2025 12th Iranian Conference on Renewable Energies and Distributed

- Generation (ICREDG), Qom, Iran, Islamic Republic of, 2025, pp. 1-6, doi: 10.1109/ICREDG66184.2025.10966107.
- [21] D. Casadei, G. Grandi, A. Lega, and C. Rossi, "Multilevel operation and input power balancing for a dual two-level inverter with insulated DC sources," IEEE Trans. Ind. Appl., vol. 44, no. 6, pp. 1815–1824, 2008, doi: 10.1109/TIA.2008.2006323.
- [22] F. Hong, J. Liu, B. Ji, Y. Zhou, J. Wang and C. Wang, "Interleaved Dual Buck Full-Bridge Three-Level Inverter," in IEEE Transactions on Power Electronics, vol. 31, no. 2, pp. 964-974, Feb. 2016, doi: 10.1109/TPEL.2015.2421295.
- [23] R. Shi, S. Semsar and P. W. Lehn, "Constant Current Fast Charging of Electric Vehicles via a DC Grid Using a Dual-Inverter Drive," in IEEE Transactions on Industrial Electronics, vol. 64, no. 9, pp. 6940-6949, Sept. 2017, doi: 10.1109/TIE.2017.2686362.
- [24] Z. Bai, H. Ma, D. Xu, B. Wu, Y. Fang, and Y. Yao, "Resonance damping and harmonic suppression for grid-connected current-source converter," IEEE Trans. Ind. Electron., vol. 61, no. 7, pp. 3146–3154, 2014, doi: 10.1109/TIE.2013.2281173.
- [25] K. Basu, A. K. Sahoo, V. Chandrasekaran, and N. Mohan, "Grid-Side AC line filter design of a current source rectifier with analytical estimation of input current ripple," IEEE Trans. Power Electron., vol. 29, no. 12, pp. 6394–6405, 2014, doi: 10.1109/TPEL.2014.2305435.
- [26] M. H. Shaabani, N. Dehghan, M. H. Nemati and B. Vahidi, "Improvement of DC Power Response Using Artificial Neural Network in an Off-Grid PV System Linked to a Constant Power Load," 2024 11th Iranian Conference on Renewable Energy and Distribution Generation (ICREDG), Yazd, Iran, Islamic Republic of, 2024, pp. 1-6, doi: 10.1109/ICREDG61679.2024.10607824.
- [27] H. Karneddi, D. Ronanki and J. Rodriguez, "Universal Integrated Onboard Charger With Model Predictive Current Control for Plug-In EV Charging," in IEEE Transactions on Power Electronics, vol. 40, no. 1, pp. 28-33, Jan. 2025, doi: 10.1109/TPEL.2024.3428855.
- [28] L. Tan, B. Wu, V. Yaramasu, S. Rivera and X. Guo, "Effective Voltage Balance Control for Bipolar-DC-Bus-Fed EV Charging Station With Three-Level DC-DC Fast Charger," " in IEEE Transactions on Industrial Electronics, vol. 63, no. 7, pp. 4031-4041, July 2016, doi: 10.1109/TIE.2016.2539248.